The Astronomical Journal, 171:206 (8pp), 2026 April https://doi.org/10.3847/1538-3881/ae43e4

Exoplanet Synchronization in the Habitable Zone: Learning from Venus' Retrograde Rotation

Sylvio Ferraz-Mello
Institute of Astronomy, Geophysics and Atmospheric Sciences, Universidade de São Paulo, Brazil; sylvio@iag.usp.br
Received 2025 December 30; revised 2026 February 6; accepted 2026 February 9; published 2026 March 6

Abstract

The rotation of a planet in the habitable zone (HZ) of a solar-type star may be reversed by a smooth process associated with the formation of its atmosphere and the emergence of torques stronger than and opposite to the normal tidal torques. Our understanding of Venus' rotational dynamics is revisited to look at what might happen to exoplanets in the HZ of a solar-type star. Current theories are used to construct a simplified model of the joint contribution of the gravitational tidal torque and the atmospheric torque. It shows that the reversal of a planet's rotation is not an exceptional fact and may have happened many times amongst the known HZ exoplanets.

Unified Astronomy Thesaurus concepts: Tidal friction (1698); Atmospheric tides (118); Venus (1763); Planetary science (1255); Habitable zone (696); Extrasolar rocky planets (511)

1. Introduction

This paper aims to use our knowledge of Venus' rotation as insight into what to expect for the rotation of Earth-like exoplanets in the habitable zone (HZ) of a solar-type star. It reviews various published results and compares them to hypothetical situations to improve our understanding of their implications. It includes a new discussion of the existence and stability of stationary solutions under the joint actions of tidal and atmospheric torques. When the eccentricity is neglected, these solutions might be synchronous or asynchronous (a.k.a. parasynchronous), stable or unstable (A. C. M. Correia & J. Laskar 2001, 2003a; A. C. M. Correia et al. 2003; J. Leconte et al. 2015; P. Auclair-Desrotour et al. 2017). Two parameters representing the ratios of tidal and atmospheric torques are introduced, along with a toy model. They allow us to study several different evolutionary paths for the rotation of exoplanets located in the HZ of solar-type stars. In these cases, the HZ is not too close to the star, and planets may harbor dynamically significant atmospheres. Exploration of the model shows that the evolution leading to a retrograde rotation can happen at a slow pace and is not a low-probability event. The retrograde rotation of Venus may be the result of a smooth, deterministic process associated with the formation of its atmosphere, rather than a collisional process that suddenly transferred a huge amount of negative angular momentum to the planet. The collisional processes often used to explain the retrograde rotation of Venus (T. B. McCord 1968; V. V. Makarov & A. Goldin 2023) are not the only possibilities. The smooth process proposed in this paper was first described by A. C. M. Correia & J. Laskar (2003b). Though it is not the only way to reverse the rotation of a planet, it is simple, realistic, and does not depend on exceptional conditions, such as high eccentricity or obliquity.

In Section 2, we present the main data on Venus' rotation, and the new, full 3D version of the creep tide theory (H. Folonier et al. 2025) is used to determine how long the retrograde rotation can resist the action of the tidal torque. In Section 3, we introduce the torque due to the phase lead of the atmospheric bulge, and investigate the main effects due to the joint actions of the atmospheric and tidal torques. In Section 4, we show how the evolution of the atmosphere can cause the reversal of the planet's rotation from direct to retrograde. A toy model for the planet rotation provides evolutionary examples of this process. Section 5 collects the main conclusions of the paper. An Appendix is included, showing that using the classical Darwin's tidal theory to calculate the tidal torque yields the same results as the creep tide theory.

2. Venus' Rotation

Venus currently has a retrograde rotation with a period of 243.0226 ± 0.0013 days (J.-L. Margot et al. 2021). We know that this rotation is strongly affected by the thermal bulges in the planet's atmosphere. How would a retrograde rotation of this kind evolve should the planet be devoid of an atmosphere? We have investigated this topic using the new version of the creep tide theory valid for systems with a nonzero obliquity (H. Folonier et al. 2025).

2.1. Back to Prograde

The main result is that the rotation of a naked Venus would become prograde in a relatively short time (see Figure 1). Using typical values for Venus' parameters involved in this calculation (see Table 1), the result is an inversion in $\sim$700,000 yr if the relaxation is $\gamma \sim 2 \times 10^{-7}\,\mathrm{s}^{-1}$ (as for the solid Earth; see S. Ferraz-Mello 2013). Tidal theory also indicates that, at the inversion, we do not have a reversal of the rotation but a continuous migration of the rotation poles, which are displaced until the inversion is completed. During the inversion interval, the angular momentum of the planet is very small (the rotation period increases to several thousand days). We do not know if the planet itself would turn upside down because the equations of the polhode are not included in the model. After the reversal of the rotation back to a prograde state, the rotation accelerates and is driven to a stable synchronization with the orbital period (see Figure 1, right).

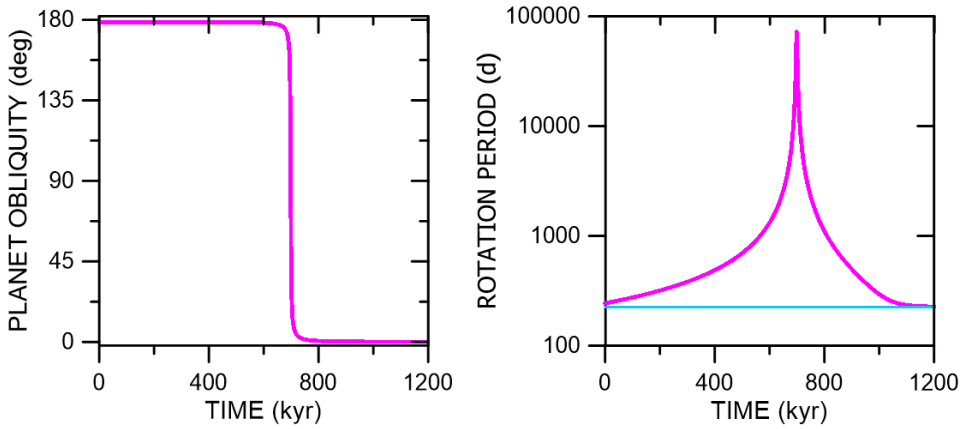

Figure 1. Rotation reversal. Left: tidal reversal of the planet obliquity. Right: evolution of the rotation period (red) and the orbital period (blue).

Table 1
Venus Dynamic Parameters

Mass (M)	0.815 Earth mass
Radius (R)	0.949 Earth radius
Rotation period	243.0226 days (R)
Oblateness	6.64×10^{-6}
Axial tilt with respect to the ecliptic pole (J)	175°.7
Obliquity	178°.3933
Moment of inertia (C)	$0.34\,MR^2$
Tidal relaxation factor (γ)	2×10^{-7} s^{-1}
Tidal Love number (k_2)	0.295
Semimajor axis	0.7238 au
Orbital period	224.9145 days
Eccentricity	0.006773
Inclination	3°.395
Length of the day	116.8091 days
Atmospheric bulge lead (σ')	30°–34°
Semidiurnal frequency (ν)	-1.245144×10^{-6} s^{-1}

2.2. The Rotation Phase Diagram

In the zero-obliquity version (a.k.a. the coplanar version) of the tidal theory, the average variation of the rotation of the planet is given by the first-order differential equation (S. Ferraz-Mello 2013; A. C. M. Correia et al. 2014; S. Ferraz-Mello et al. 2022):

$$\langle \dot{\Omega} \rangle = -A \sum_{k \in Z} E_{2,k}^2 \sin 2\sigma_k, \tag{1}$$

where

$$A = \frac{3k_2 GM^2 R^5}{4Ca^6} \tag{2}$$

is a positive coefficient depending on the dynamical parameters of the system, where G is the gravitational constant, M the mass of the central star, R the planet radius, C its moment of inertia, k_2 the tidal Love number, and a the orbital semimajor axis. $E_{2,k}$ are known functions of the orbital eccentricity e (Cayley polynomials), and σ_k are the angular lags of the components of the tide, defined in the interval $(-\pi/2, +\pi/2)$, by the functions

$$\tan \sigma_k = \frac{\nu + kn}{\gamma}, \tag{3}$$

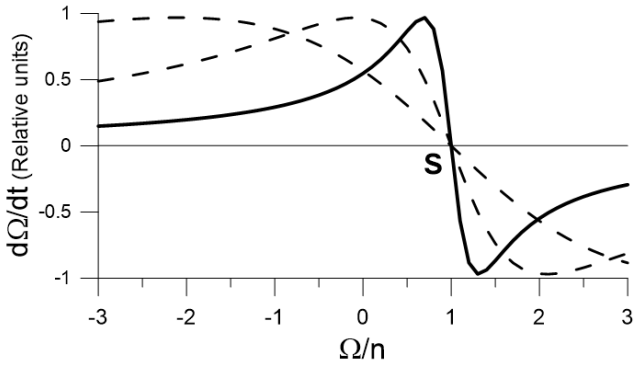

Figure 2. Phase diagram for $e = 0.006773$ and relaxation factors 2×10^{-7} s^{-1} (solid line), 7×10^{-7} s^{-1} and 2×10^{-6} s^{-1} (dashed lines).

where $\nu = 2\Omega - 2n$ is the semidiurnal frequency. Hence,

$$\sin 2\sigma_k = \frac{2\gamma(\nu + kn)}{\gamma^2 + (\nu + kn)^2}. \tag{4}$$

In the circular approximation, the only remaining term is $k = 0$, and σ_0 is the lag of the main tidal component: the semidiurnal tide.

Figure 2 shows a plot of the function $\langle \dot{\Omega} \rangle = f(\Omega)$ for a wide range of rotation velocities of a naked Venus. It shows that, for the current orbital eccentricity, there is only one stationary solution S, at $\Omega/n \simeq 1$. This solution is stable since $\dot{\Omega}$ is positive on the left of S and negative on its right. This situation is robust and is confirmed for a wide range of variations in the parameters involved in the function $f(\Omega)$.

3. The Atmospheric Torque

The retrograde rotation of Venus could not persist for a long time if the gravitational tidal torque was the only one acting on the planet. The observed retrograde rotation is a clear indication of the existence of a torque acting in the opposite direction. This has been attributed to a phase lead in the thermal deformation of the atmosphere (T. Gold & S. Soter 1971; A. P. Ingersoll & A. R. Dobrovolskis 1978).[1]

Solar attraction also produces deformations in the atmosphere of Venus, giving rise to an additional torque that acts to slow the

[1] For detailed discussions of this model, see A. C. M. Correia & J. Laskar (2003a), J. Leconte et al. (2015). P. Auclair-Desrotour et al. (2017, 2024), and references therein.

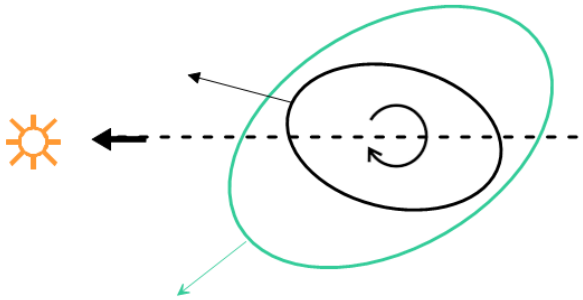

Figure 3. The atmospheric and tidal bulges in a system of reference in which the direction of the Sun is kept fixed. See A. P. Ingersoll & A. R. Dobrovolskis (1978).

planet's rotation (A. R. Dobrovolskis 1980; E. F. S. Valente & A. C. M. Correia 2023). However, in the absence of a significant obliquity, it is weaker and is not considered in the present study.

Solar radiation raises the air temperatures in the afternoon and causes the air mass to flow to colder regions. In a first approximation, the atmosphere may be represented by an ellipsoid whose bulge is displaced in the direction contrary to the rotation of the body (see Figure 3). In this figure, the direction of the orbital motion does not matter. The rotation direction indicated is not absolute, but relative to the Sun's direction. At one given point on the planet's surface, the tidal bulge is felt after noon. The gravitational tide is delayed. In contrast, the atmospheric bulge leads the rotation. The gravitational attraction of the Sun on the atmosphere introduces a torque in a direction opposite to that of the gravitational tide.

Using notations similar to those adopted in the previous section, the contribution of the atmospheric bulge to the rotation of the planet is

$$\dot{\Omega} = A' \sin 2\sigma', \tag{5}$$

where

$$A'\gamma' = \frac{3\pi n^2 R^4 \Phi_0}{8 c_p T_0 C} \tag{6}$$

is a positive coefficient depending on the mean motion (n), the radius (R), the moment of inertia (C), the temperature at the surface (T_0), its specific heat at constant pressure (c_p), and on the heat flux at the subsolar point (Φ_0),[2] and where σ' is the lead of the atmospheric bulge, defined by

$$\tan \sigma' = \nu\tau' \equiv \frac{\nu}{\gamma'} \tag{7}$$

(A. P. Ingersoll & A. R. Dobrovolskis 1978), where τ' is a proportionality constant and $\gamma' = 1/\tau'$. A' has the same dimension as A. Note that when $e = 0$, Equations (1) and (5) are formally equal. As before, the angle σ' is defined by the principal value of the function in the interval $(-\pi/2, +\pi/2)$. In the case of Venus, the maxima of the atmospheric pressure are recorded at 09:45 and 22:00 local solar time (see P. Auclair-Desrotour et al. 2024). This means $\sigma' \sim 32°$.

[2] This coefficient formally differs from the coefficient appearing in A. P. Ingersoll & A. R. Dobrovolskis (1978) by a factor 2. The division by 2 is here necessary to compensate for the factor 2 present in the expression of $\sin 2\sigma'$.

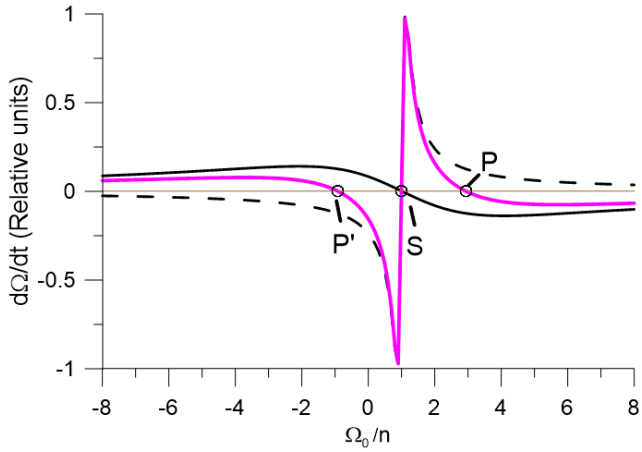

Figure 4. Phase diagram $\dot{\Omega}(\Omega)$ resulting from the composition (red) of the tidal (solid black) and atmospheric (dashed) torques. The intersections of the red curve with the axis $\dot{\Omega} = 0$ (brown) are the stationary solutions: The unstable synchronous solution S and two stable asynchronous solutions P and P′, one prograde and one retrograde. The adopted factors γ and γ' were exaggerated to improve the visibility of the plot's main features.

3.1. The Composite Phase Diagram

Under the assumptions of zero obliquity and zero eccentricity, the variation of the rotation of the planet is described by an autonomous first-order differential equation formed by the composition of Equations (1) (for $e = 0$) and (5):

$$\dot{\Omega} = -A \sin 2\sigma_0 + A' \sin 2\sigma' \tag{8}$$

or

$$\dot{\Omega} = A \sin 2\sigma_0 \left(b \quad \frac{\nu^2 + \gamma^2}{\nu^2 + \gamma'^2} - 1 \right), \tag{9}$$

where

$$b = \frac{A'\gamma'}{A\gamma}. \tag{10}$$

The parameter b is akin to the ratio of the two torques. It equals 0 in the absence of atmospheric torque and increases with the influence of atmospheric torque. It plays a critical role in the existence and stability of stationary solutions.

The red curve in Figure 4 plots the resulting function $\dot{\Omega}(\Omega)$ in arbitrary units (such that the largest elongation of the function is equal to 1). The figure also shows the individual contribution of the two terms of Equation (8): the tidal torque (black solid line) and the atmospheric torque (dashed line).

The intersections of the red curve with the axis $\dot{\Omega} = 0$ are stationary solutions of the system. One of these solutions, S, lies at $\Omega/n = 1$ and is a synchronous solution. A simple analysis of the sign of $\dot{\Omega}$ on the right and left of this point indicates that this solution is unstable. The derivative of the curve $\dot{\Omega}(\Omega)$ in the neighborhood of the crossing point is positive. One may note that in the component corresponding to the tide of a naked planet (black solid line), the sign is negative, indicating the stability of the synchronous solution in that case.

The figure shows two more intersections at the points P and P′. The derivative of the functions at these two crossings of the axis $\dot{\Omega} = 0$ is negative, so both correspond to stable stationary solutions. These two asynchronous solutions are symmetric

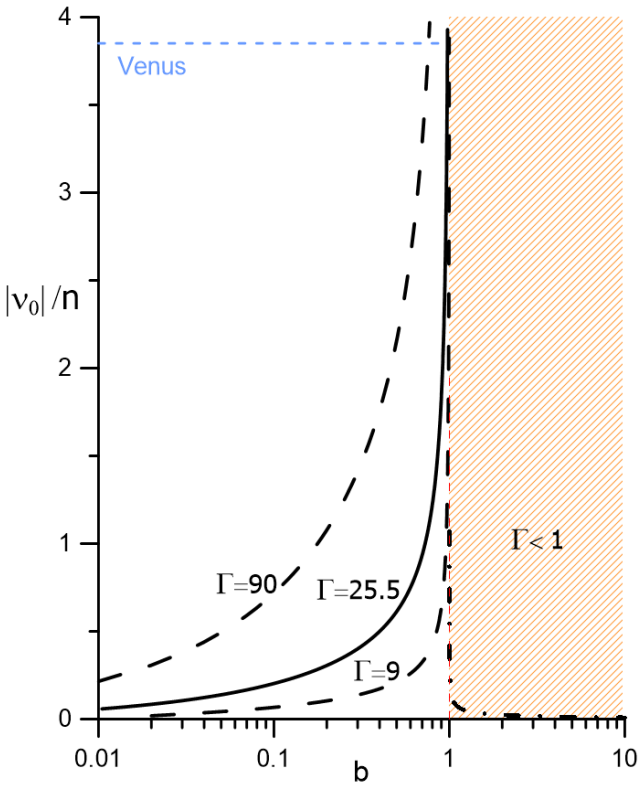

Figure 5. Loci of the asynchronous stationary solutions for given values of Γ. These solutions are stable if they fall in the zone $b < 1$ and unstable otherwise. If $|\nu_0/n| < 1$, they are both prograde. If $|\nu_0/n| > 1$, one is prograde and the other is retrograde.

with respect to the synchronous solution and, in the case shown in Figure 4, the solution at P is prograde and the solution at P′ is retrograde.

In the case of Venus, the figure is similar to Figure 4. However, the excursion of the function $\dot{\Omega}(\Omega)$ near the synchronous solution is too large and, keeping the figure at scale, the red lines near the asymmetric solutions and the axis $\dot{\Omega} = 0$ are indistinguishable, leaving the crossings invisible (even if they are well defined in the data file). To make them visible, the factors γ and γ' adopted in the construction of Figure 4 were multiplied by 10.

3.2. Existence and Stability of the Asynchronous Solutions

The bracket in Equation (9) can be expressed as the quotient of two polynomials in ν, and equation $\dot{\Omega} = 0$ has the same roots as the symmetric third-degree polynomial in the numerator. One of these roots is $\nu_0 = 0$, and the other two are given by

$$\nu_0^2 = \gamma'^2 \quad \frac{1 - b\Gamma^2}{b - 1}, \tag{11}$$

where

$$\Gamma = \frac{\gamma}{\gamma'}. \tag{12}$$

The condition for the existence of real roots $\pm\nu_0$ is that the numerator and denominator are simultaneously positive or negative (otherwise, we get $\nu_0^2 < 0$ and the two roots are imaginary):

Case I: $\Gamma^{-2} < b < 1 \quad (\Gamma > 1)$;

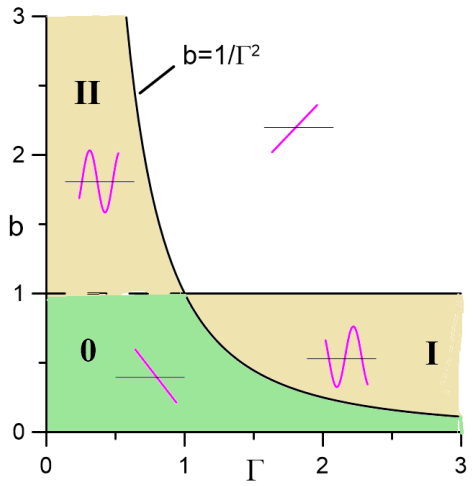

Figure 6. Domains of existence of the asynchronous stationary solutions: I stable, II unstable. Outside these domains, they are not real. In domains 0 and II, the synchronous stationary solution is stable. In other domains, it is unstable. The inserted sketches show how the roots are formed in each domain.

Case II: $1 < b < \Gamma^{-2} \quad (\Gamma < 1)$.

Otherwise, the two roots are imaginary.

The analysis of the behavior of $\dot{\Omega}(\Omega)$ when $|\Omega| \to \infty$ allows us to conclude that, in case I, the synchronous root is unstable and the two asynchronous roots are stable (as shown in Figure 4). In case II, the behavior is inverted, the synchronous root is stable, and the two asynchronous roots are unstable.

These stationary solutions are similar to those found by P. Auclair-Desrotour et al. (2017) using a Maxwell rheology.

The loci of the asynchronous solutions for given values of Γ are shown in Figure 5.

3.3. Stability of the Synchronous Solutions

In domains I and II the synchronous solution is unstable when the asynchronous solutions are stable, and vice versa. In the other domains, the synchronous solution is the only real root. The stability is again deduced from the study of the leading term of the third-degree polynomial that defines the roots: $\dot{\Omega} = \text{const} \cdot (b - 1)\nu^3 + \cdots$ [3] The synchronous solution is stable when $b < 1$ and unstable otherwise. This is consistent with the plots of the partial contributions of the tidal and atmospheric torques shown in Figure 4.

In the domain 0 (green area) of Figure 6, the tidal torque is dominant and the synchronous solution is stable as in the case of a naked Venus. In the white area, the atmospheric torque is dominant, and the synchronous solution is unstable.

4. The Evolution Toward a Retrograde Rotation

In the general case, planets are assumed to rotate prograde (see L. Dones & S. Tremaine 1993; E. Kokubo & S. Ida 2007). Figure 4 shows that in case I, it is impossible for the rotation to evolve smoothly to a retrograde condition. The space between the parasynchronous solutions P and P′ acts as a wall that prevents one solution starting on the right-hand side (prograde) from reaching the left-hand side of the diagram. The same

[3] The function is of the kind $y' = y.f(y)$. The stability of the root $y = 0$ may be inferred from the study of a finite interval.

situation is repeated more or less in the other cases. For this reason, we often read that some collisional event may have been the cause of Venus' retrograde rotation, the most realistic being related to the transfer of negative angular momentum from a retrograde satellite (see, e.g., T. B. McCord 1968; V. V. Makarov & A. Goldin 2023).

However, the impossibility mentioned above results from considering a frozen model. Inspection of Figure 6 shows that, if we accept that the physical conditions are certainly not frozen, and the relative contribution of the tidal and atmospheric torques may have differed in the past, it is possible to have paths leading smoothly from a prograde rotation in the past to an asynchronous retrograde rotation in the present. We may, for example, consider an evolution path starting in domain 0 (green area) of Figure 6 and crossing the frontier between it and domain I. In domain 0, the rotation will evolve toward the synchronous solution and will reach it if enough time is allowed for the path segment inside domain 0. When crossing the boundary toward domain I, the synchronous solution becomes unstable, and the rotation is forced to evolve toward one of the two new stable asynchronous solutions. If the rotation is synchronous before the crossing, there is no mathematical reason to privilege one of the two solutions, and the probabilities of evolving toward P or P′ are equal. However, the increase in the moment of inertia due to the transfer of mass from the planet's core to its atmosphere may create a bias in favor of the branch leading to retrograde rotation.

If the atmosphere of Venus is still changing, the current rotational state of Venus can change. For instance, if we assume that Venus' rotation is currently trapped in a retrograde asynchronous stationary solution, we get $b = 0.97489$, which is very close to the boundary $b = 1$. A small change, say, in the surface temperature of Venus may result in b increasing to $b > 1$. Consequently, stable asynchronous stationary solutions cease to exist, and the rotation of Venus will increase continuously.

In fact, we cannot a priori exclude the possibility that the rotation of Venus is already in such a state of runaway increase. Measurements of Venus' rotation period are difficult, and the available data (see J.-L. Margot et al. 2021) do not rule out a very slow increase.

4.1. Smooth Transitions in a Toy Model

We rewrite Equation (9) with the modified dependent variable

$$y = \frac{\nu}{\gamma'} \tag{13}$$

and the positive coefficient

$$D = \frac{4A\Gamma}{\gamma'}. \tag{14}$$

Hence,

$$\dot{y} = D \quad \frac{(b-1)y^3 + (b\Gamma^2 - 1)y}{(y^2+1)(y^2+\Gamma^2)}. \tag{15}$$

Figure 7 shows a solution for this equation along a path defined by $b = \Gamma/64$ with initial conditions $y(0) = 3$ and $D = 10$. This path is arbitrary, starts at the origin $b = 0$, $\Gamma = 0$ (absence of atmosphere), and evolves linearly as the atmosphere is formed. It crosses the boundary of domains 0 and I when $\Gamma = 4$, and reaches the domain $b \geqslant 1$ when $\Gamma = 64$. The following features may be observed: While $\Gamma < 4$, y decreases, tending to the synchronous solution $y = 0$, which is not reached; when $\Gamma = 4$, the solution $y = 0$ becomes unstable, and y evolves away from it. In the first segment, the increase is exponential (we have $\dot{y} \simeq y$). It approaches the stationary solution P. Since the parameters b and Γ are continuously changing, the position of this solution changes (see the dashed line). It is not reached exactly. The actual solution oscillates around it. Nothing is seen when the boundary $b = 1$ is crossed. The rotation velocity continues to increase at the same pace as before.

If the initial condition is taken as negative, the result is the same upside down. Equation (15) can be written as $\dot{y} = yF(y, t)$, and it is easy to see that no solution can cross the line $y = 0$. If at a given moment $y = 0$, it will remain equal to 0 forever.

The toy model can be improved by taking into account that the atmosphere is formed through the planet's outgassing. Consequently, mass is transferred from the planet's interior to the atmosphere. This process increases the system's moment of inertia. The effect of a small uniform increase in the planet's moment of inertia is a small subtractive term, $-Z$, in dy/dt. Hence,

$$\dot{y} = D \quad \frac{(b-1)y^3 + (b\Gamma^2 - 1)y}{(y^2+1)(y^2+\Gamma^2)} - Z, \tag{16}$$

where Z is proportional to the rate of deceleration of the planet's rotation.

The left panel of Figure 8 shows the initial part of one solution for this equation obtained with the same parameters and initial conditions as before for $Z = 10^{-3}$. In this solution, y becomes negative as soon as the solution approaches the synchronous stationary solution, still inside the domain 0. The rotation becomes subsynchronous (i.e., $\nu < 0$, or $\Omega < n$) and, later on, becomes retrograde. We stress the fact that what is being observed in Figure 8 is not the transition from prograde to retrograde, but the transition from supersynchronous ($\Omega > n$) to subsynchronous ($\Omega < n$). However, as $|\nu|$ increases, it can become larger than $2n$, and hence $\Omega < 0$.

The right panel of Figure 8 shows an alternative path, in which b increases more rapidly than Γ ($b = 2, 5\Gamma$). While in the previous case the increase in the angle σ' led the evolution, here that angle changes slowly, and the evolution is ruled by the increasing coefficient A', which means stronger atmospheric tides. The path goes from domain 0 to domain II (instead of domain I), but later on it crosses the boundary $b = \Gamma^{-2}$ and enters the white region where no stable stationary solution exists. y remains near the synchronous solution for a while, but eventually starts a runaway increase to negative values. The rotation becomes subsynchronous (i.e., $\nu < 0$, or $\Omega < n$) and evolves toward a retrograde one.

5. Conclusion

The main result of this paper is that no collision with other bodies is necessary to convert the rotation of an Earth or super-Earth with a significant atmosphere formed in the course of its evolution into a retrograde rotation. It is enough for the planet to be at a distance from the host star short enough for tidal torques to nearly synchronize the rotation of the planet before the bulk of its atmosphere forms (but not so close that the stellar radiation destroys the formed atmosphere). As the

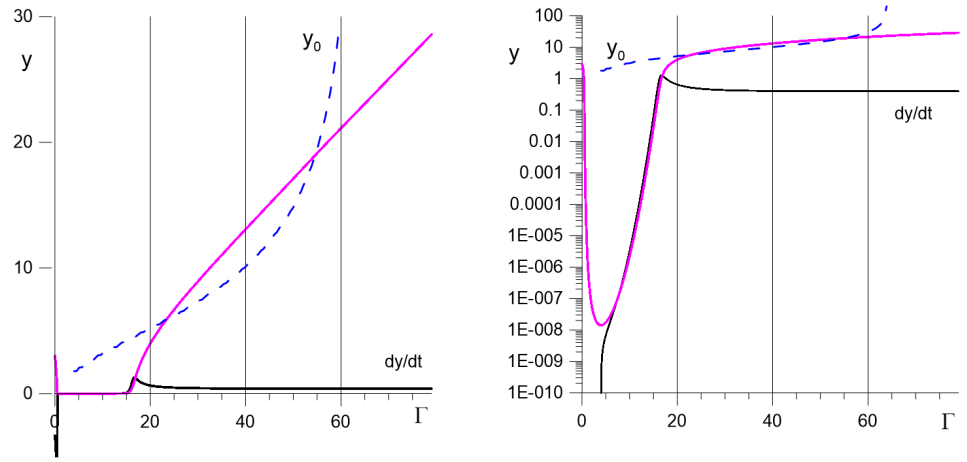

Figure 7. Left: the solution of Equation (15) along a path defined by $b = \Gamma/64$ crossing the regions 0 and I of Figure 6 before reaching the boundary $b = 1$. Right: the same is shown only with a logarithmic scale. Also shown are the locus of the stationary root $y_0 = \nu_0/\gamma'$ (dashed line) and the derivative dy/dt (black).

atmosphere forms from the outgassing of the planet, the transfer of mass from the planet to its atmosphere may cause a loss of angular velocity, so that the rotation is subsynchronous when the atmospheric torques become more important than the tidal torques.[4] Subsequently, the prevailing atmospheric torques increase the planet's relative rotation, eventually allowing it to become retrograde. None of these processes involves a catastrophic event (even if the transformation of a stable stationary solution into an unstable one is a typical example of René Thom's catastrophes; see V. Arnold 1984). The formation of the planetary atmosphere is a continuous, smooth process, which may be more or less efficient but is not a low-probability event.

The examples constructed using a toy model in Section 4.1 introduced planet evolution histories in which the parameters b and Γ increase uniformly. This choice is only justified by its simplicity. The mathematical phenomena shown in that example do not depend on the adopted path. The essential points are that the system must remain in domain 0 for long enough for it to reach near synchronization, and then cross the boundary $b = 1/\Gamma^2$, where the nature of the synchronous solution changes from stable to unstable. The shift to retrograde is not a necessary fate, and depends on the sign of ν just before crossing. If the motion is still super-synchronous, it will remain prograde forever. Conversely, if it is subsynchronous, it may evolve toward a retrograde rotation.

The conclusions are based on simplified models, but they are robust and unlikely to change if different tidal models are used (see A. C. M. Correia & J. Laskar 2003b; A. C. M. Correia et al. 2003). The gravitational tidal torque creates one stationary synchronous solution at $\nu \simeq 0$ so long as the eccentricity of the orbit is kept small. The existence of a contrary torque maintains the current retrograde rotation of Venus. Improvements in the atmospheric torque model should not change the fact that, acting alone, it creates an unstable synchronous solution. When the two torques act together, they lead to a synchronous solution that is stable as long as the gravitational tidal torque dominates and unstable otherwise. The result is a mere consequence of these model-independent facts.

[4] Keep in mind that subsynchronous means $\nu < 0$ and retrograde means $\Omega < 0$.

The toy model introduced in Section 3.1 owes its simplicity to the assumption of zero eccentricity and to the coplanarity of the planet's orbit and equator. If we consider orbits with significant eccentricity, even while retaining the coplanarity hypothesis, many other equilibrium solutions appear. In the case of a planet without an atmosphere, they are the well-known spin–orbit resonances $\Omega/n = k/2$ ($k = 1, 3, 4, \cdots$), with the number of resonances increasing for larger eccentricities (see A. C. M. Correia et al. 2014; S. Ferraz-Mello 2015). If, in addition, we have a nonzero obliquity, the scenario becomes yet more complex. It is then difficult to construct a general model, and it is preferable to consider particular cases, as in the extended study of the stationary solutions of Kepler 1229 b done by E. F. S. Valente et al. (2024).

The planet's dense atmosphere plays a role not only in the inversion of its rotation but also in maintaining its retrograde state. The study of a naked Venus shows that, in the absence of atmospheric torque, the current retrograde rotation would revert to prograde in less than one million years. The full 3D creep tide theory indicates that, at this inversion, the rotation does not undergo a simple reversal, but instead the rotation poles migrate continuously and are displaced until the inversion is complete.

Acknowledgments

This investigation was sponsored by CNPq (Proc. 303540/2020-6) and FAPESP (Proc. 2016/13750-6; ref. PLATO mission). Part of this research was conducted at the Southwest Research Institute in Boulder. I thank Dr. R. Alves-Silva and the referee for their suggestions and comments.

Appendix
Comparison with Results Obtained with Darwin's Theory

The use of different tidal theories led to results (J. Leconte et al. 2015) indicating that synchronous solutions are always stable. This is a crucial question, since in such cases it is impossible to obtain results like those shown in the previous section, in which the rotation may become subsynchronous, and eventually retrograde, after crossing a critical boundary where a pitchfork bifurcation occurs. In this appendix, we show that, for circular orbits, Darwin's theory for viscous planets and the creep tide theory coincide, and that other Darwinian approaches do not lead to different results from

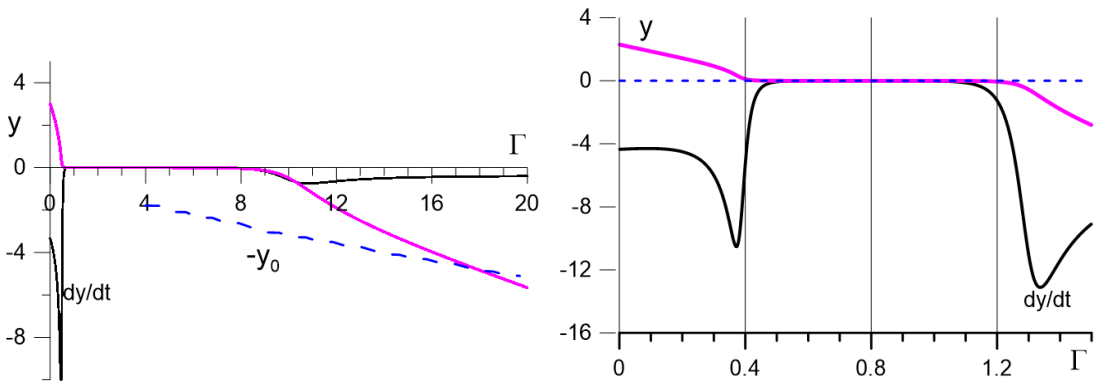

Figure 8. Solution of Equation (16). At $t = 0$ ($\Gamma = 0$), the rotation is prograde. Near synchronization, it changes from supersynchronous ($y > 0$) to subsynchronous ($y < 0$). Subsequently, it becomes retrograde. Left: the same path as Figure 7. Right: an alternative along a path that drives the solution from domain 0 to domain II, instead of domain I, and eventually to the white domain where the synchronous rotation is unstable. In both cases, $Z = -10^{-3}$.

those found using creep tide theory to calculate the tidal variation of the rotation speed.

The use of a plugged ad hoc lag instead of a lag calculated from first principles is a simplification introduced by Darwin himself (G. H. Darwin 1880). The starting point in the theories referred to currently as "equilibrium tide theories" is a static tide. A dynamic tide is assumed to be generated by the same harmonics as the static tide, each delayed by a given phase delay, ε_k (see S. Ferraz-Mello 2019). Additionally, each term is assumed to have an amplitude attenuation equal to the cosine of the corresponding phase delay. In Darwin's words, "In a frictional fluid, the tide will be reduced in height and altered in phase." (G. H. Darwin 1880, Section 4).

If the weak-friction approximation is *not* used,[5] the average contribution of the tides to the planet rotation (see S. Ferraz-Mello et al. 2008) becomes

$$\langle \dot{\Omega} \rangle = -\frac{3k_2 GM^2 R^5}{4Ca^6} \sin 2\varepsilon_0 \equiv -A \frac{2\tan\varepsilon_0}{1+\tan^2\varepsilon_0} \qquad \text{(A1)}$$

in the circular approximation.

A.1. Darwin's Theory for a Viscous Planet

In the case of a viscous planet, the plugged ad hoc lag is

$$\varepsilon_0 = \arctan \tau\nu,$$

where τ is a constant (G. H. Darwin 1880, Section 7), and the tidal variation of the planet's rotational velocity is

$$\langle \dot{\Omega} \rangle = -A \frac{2\tau\nu}{1+\tau^2\nu^2}. \qquad \text{(A2)}$$

If we set $\tau = \frac{1}{\gamma}$, this equation is transformed into the same equation obtained with the creep tide theory in the circular approximation. Therefore, the stationary solutions for the rotation of a planet under the joint actions of the gravitational and atmospheric tides are the same as those given in Section 3.

[5] The "weak-friction approximation," introduced by H. Gerstenkorn (1955), assumes that the lags (ε_k) are small, allowing the simplifications $\sin\varepsilon_k = \varepsilon_k$ and $\cos\varepsilon_k = 1$. These apparently harmless modifications introduce essential changes in the theory, and are at the origin of several conceptual difficulties (see M. Efroimsky & J. G. Williams 2009 Section 9.4).

A.2. The Maxwell and Andrade Rheologies

The general Equation (A2) may be written as

$$\langle \dot{\Omega} \rangle = -2A\left(\tan\varepsilon_0 + \frac{1}{\tan\varepsilon_0}\right)^{-1}, \qquad \text{(A3)}$$

or, using Darwin's approach for viscous planets,

$$\langle \dot{\Omega} \rangle = -2A\left(\tau\nu + \frac{1}{\tau\nu}\right)^{-1}. \qquad \text{(A4)}$$

The function

$$Q = \left(\tau\nu + \frac{1}{\tau\nu}\right) \qquad \text{(A5)}$$

appears frequently in the existing literature on planetary tides and is referred to as the *quality factor* (see S. Ferraz-Mello 2015). It carries an interpretation related to the energy dissipation in the system and is characteristic of Maxwell rheology. Figure 9 is the well-known log–log plot of $1/Q$ as a function of $\tau\nu$ for Maxwell rheology. If no logarithmic scales are used, the figure is exactly equal to the curves in the phase diagram shown in Figure 2 (in an arbitrary scale).

Laboratory studies indicate that solid bodies do not follow Maxwell rheology when $|\tau\nu| \gg 1$, but Andrade rheology (M. Efroimsky 2012a; Y. Gevorgyan et al. 2020). However, when Andrade rheology is adopted, the results are comparable to those of the Darwin theory and creep tide theory, with their intrinsic Maxwellian rheology. The only difference lies in the fact that the descending branch of Andrade rheology will show an elbow and, after it, a slower decay (as shown by the blue line of Figure 9). Consequently, the slow decay of the tidal component $|d\Omega/dt|$ for larger $|\nu|$ (see Figure 4) will be still slower. However, the interval between the maximum and minimum of $|d\Omega/dt|$ will not be affected (since it corresponds to the ascending branch, which is the same in both rheologies). We may conclude that the asynchronous solutions in the case shown in Figure 4 are the same in both Andrade and Maxwell rheologies.

A.3. The Constant Time Lag and Constant Phase Lag Theories

Two widely used versions of Darwin's theory are the constant time lag (CTL) and the constant phase lag (CPL) theories (see R. Greenberg 2009; R. Barnes 2017).

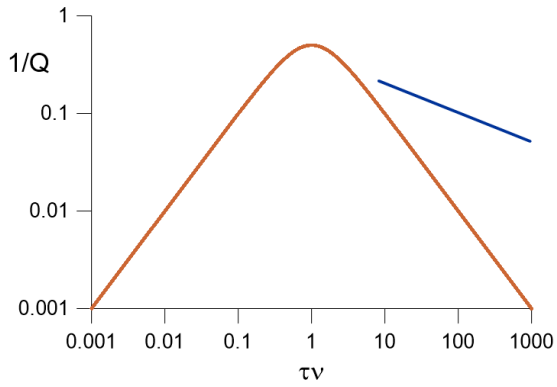

Figure 9. Maxwell rheology. Log–log plot of the inverse of the quality factor Q as a function of $\tau\nu$. The blue line shows the slope of the descending branch in the case of Andrade rheology with $p = -0.2$.

In the circular approximation of the CTL model, the plugged lag is a quantity proportional to the semidiurnal frequency:

$$\varepsilon_0 = \tau\nu,$$

where τ is a constant of proportionality (time lag). The results of CTL theory coincide with the Darwin theory for viscous planets so long as $\tau\nu \ll 1$. It can be used to study the stationary synchronous solution and its neighborhood, but not elsewhere. For larger values, the two theories diverge from one another. Besides, the results of CTL show a periodicity induced by the periodic structure of $\tan \tau\nu$, which is an artifact.

In the CPL theory, the plugged lag ε_0 does not change with the rotation velocity and is discontinuous when $\nu = 0$. For this reason, it cannot be used to study the conversion of a prograde planetary rotation into a retrograde one, which is the aim of this investigation (see M. Efroimsky 2012b).

ORCID iDs

Sylvio Ferraz-Mello https://orcid.org/0000-0002-9603-2415

References

Arnold, V. 1984, Catastrophe Theory (Springer)
Auclair-Desrotour, P., Farhat, M., Boué, G., Deitrick, R., & Laskar, J. 2024, arXiv:2410.16200
Auclair-Desrotour, P., Laskar, J., Mathis, S., & Correia, A. C. M. 2017, A&A, 603, A108
Barnes, R. 2017, CeMDA, 129, 509
Correia, A. C. M., Boué, G., Laskar, J., & Rodríguez, A. 2014, A&A, 571, A50
Correia, A. C. M., & Laskar, J. 2001, Natur, 411, 767
Correia, A. C. M., & Laskar, J. 2003a, JGRE, 108, 5123
Correia, A. C. M., & Laskar, J. 2003b, Icar, 163, 24
Correia, A. C. M., Laskar, J., & de Surgy, O. N. 2003, Icar, 163, 1
Darwin, G. H. 1880, RSPT, 171, 713
Dobrovolskis, A. R. 1980, Icar, 41, 18
Dones, L., & Tremaine, S. 1993, Icar, 103, 67
Efroimsky, M. 2012a, ApJ, 746, 150
Efroimsky, M. 2012b, CeMDA, 112, 283
Efroimsky, M., & Williams, J. G. 2009, CeMDA, 104, 257
Ferraz-Mello, S. 2013, CeMDA, 116, 109
Ferraz-Mello, S. 2015, CeMDA, 122, 359
Ferraz-Mello, S. 2019, in Satellite Dynamics and Space Missions, ed. G. Baù (Springer), 1
Ferraz-Mello, S., Folonier, H. A., & Gomes, G. O. 2022, CeMDA, 134, 25
Ferraz-Mello, S., Rodríguez, A., & Hussmann, H. 2008, CeMDA, 101, 171
Folonier, H., Ferraz-Mello, S., & Alves-Silva, R. 2025, CeMDA, 137, 15
Gerstenkorn, H. 1955, ZAp, 36, 245
Gevorgyan, Y., Boué, G., Ragazzo, C., Ruiz, L. S., & Correia, A. C. M. 2020, Icar, 343, 113610
Gold, T., & Soter, S. 1971, Icar, 14, 16
Greenberg, R. 2009, ApJL, 698, L42
Ingersoll, A. P., & Dobrovolskis, A. R. 1978, Natur, 275, 37
Kokubo, E., & Ida, S. 2007, ApJ, 671, 2082
Leconte, J., Wu, H., Menou, K., & Murray, N. 2015, Sci, 347, 632
Makarov, V. V., & Goldin, A. 2023, Univ, 10, 15
Margot, J.-L., Campbell, D. B., Giorgini, J. D., et al. 2021, NatAs, 5, 676
McCord, T. B. 1968, JGR, 73, 1497
Valente, E. F. S., & Correia, A. C. M. 2023, A&A, 679, A153
Valente, E. F. S., Correia, A. C. M., Auclair-Desrotour, P., Farhat, M., & Laskar, J. 2024, A&A, 687, A47